

# Total reflection X-ray fluorescence analysis of laser-deposited solid sample material

JAS

Full  
Paper

Jörg Spanke, Alex von Bohlen, Reinhold Klockenkämper, Alfred Quentmeier\* and Dieter Klockow

*Institut für Spektrochemie und Angewandte Spektroskopie – ISAS, Bunsen-Kirchhoff-Str. 11, D-44139 Dortmund, Germany*

Received 21st February 2000, Accepted 14th April 2000  
Published on the Web 30th May 2000

Laser ablation (LA) was applied as a sampling technique for the analysis of solids by total reflection X-ray fluorescence (TXRF). The sample material ablated by a pulsed Nd:YAG laser was collected directly on a quartz glass or Plexiglas® disc commonly used as a sample carrier for TXRF. The analytical capabilities of the combined method were investigated using an improved arrangement of solid sample and TXRF carrier. The technique was applied to the analysis of metallic samples, *i.e.* Fe–Cr binaries and high-alloy steel, and non-metallic samples, *i.e.* Al–Ti ceramics, native mineral rocks and gallstones. The nanogram amounts of material deposited on the carrier were always sufficient for TXRF analysis. Quantification was performed by addition of an internal standard. Absolute detection limits for Fe and Cr in binary samples were 50–60 pg, corresponding to a mass fraction of 5–6 mg g<sup>-1</sup> assuming a 10 ng deposit. Sampling from preselected spots of mineral rocks made possible the identification of different components in granite by means of their major and minor constituents. The combined method of LA and TXRF can be used for the rapid characterization of solids on the 10 µm scale without laborious steps of sample preparation.

## 1 Introduction

Laser ablation (LA) with a pulsed laser source is a promising technique which has already found many applications in analytical chemistry<sup>1,2</sup> and material processing.<sup>3</sup> The effective sampling capability makes LA a versatile instrument for the direct analysis of solid materials and is now widely used as one of the techniques for microsampling in spectrochemical analysis. The direct sampling process involves various advantages for the analysis of solids: no extensive sample preparation, high sample throughput and the option of micro- and local analysis. Unfortunately, LA may suffer from several drawbacks, which are introduced by the thermal character of the interaction of nanosecond-laser radiation with matter and thus are inherent in the ablation process. Fractional vaporization, for instance, has to be expected and can only be minimized if the ablation process is carefully controlled or if appropriate corrections are made, *e.g.* by the method of internal standardization. Optimum conditions for analysis can be achieved when the ablation is carried out under reduced pressure in a noble gas atmosphere.<sup>4–6</sup>

As was shown in a previous paper,<sup>7</sup> the combination of LA and TXRF is a very promising technique which makes use of the capabilities of LA for simple and rapid sampling of solid matter and of TXRF for sensitive multi-element detection of microsamples.<sup>8,9</sup> Since the laser radiation can be focused on a preselected spot of some 10 µm diameter, microgram amounts can be ablated, thus offering the possibility of quantitative micro- or local analysis of compact samples. For this purpose the ablated material was collected on an optically flat quartz glass or Plexiglas® carrier as normally used for TXRF. The carrier was positioned face-to-face with the sample surface, at a distance between 2 and 5 mm above the specimen. Nanogram amounts of material collected from a single laser pulse were sufficient for quantitative TXRF analysis. The relative detection limit of 5 mg g<sup>-1</sup> as estimated for Mn in high-alloy steel<sup>7</sup> was adequate for a rough characterization of the sample investigated. The element composition of the deposit was found to be in agreement with the stoichiometric composition

of the solid material. Deviations from the expected composition were only observed for Cu–Zn binaries where successive laser pulses on the same sample spot possibly caused a fractional evaporation.<sup>7,10</sup>

Most of the material ablated by the laser pulse was re-deposited on the sample around the laser crater. Moreover, material already collected on the carrier was partially removed by shock waves of the laser plume, when successive laser shots were applied. Both effects restricted the analytical capabilities relevant for our previous arrangement. The main objective of the present work was to improve the mass transfer rate of ejected material to the carrier and hence the analytical capabilities of the LA-TXRF combination. For this purpose the geometric arrangement of sample and TXRF carrier was substantially modified. The measurements were made mainly with high-alloy steel (bulk and sheet) and with a Fe–Cr binary system. The experimental parameters relevant for the ablation and spatial distribution of material on the carrier were investigated and optimized with respect to the mass of collected deposits. The spatial distribution on the TXRF carrier was determined by a scanning electron microscope. Analytical figures of merit (precision, accuracy, detection limits) were derived after accumulation of the deposit in a set of ten successive laser shots or from single shot measurements.

## 2 Experimental

Instead of the face-to-face alignment used earlier,<sup>7</sup> the sample was mounted perpendicular to the TXRF carrier with its lower end at a minimum distance of about 1 mm above the carrier surface (Fig. 1). The radiation from a pulsed Nd:YAG laser (Model SL401, Spectron Laser Systems, Rugby, Warwickshire, UK) was focused by a quartz lens ( $f = 185$  mm) on the sample. The laser was operated at the fundamental wavelength (1.06 µm) with pulse energies in the range 9–40 mJ and a pulse length of 8 ns. The ablation was carried out in a closed chamber with an argon atmosphere (technical grade, purity >99.998 vol.%) under reduced pressure (20–500 hPa). The

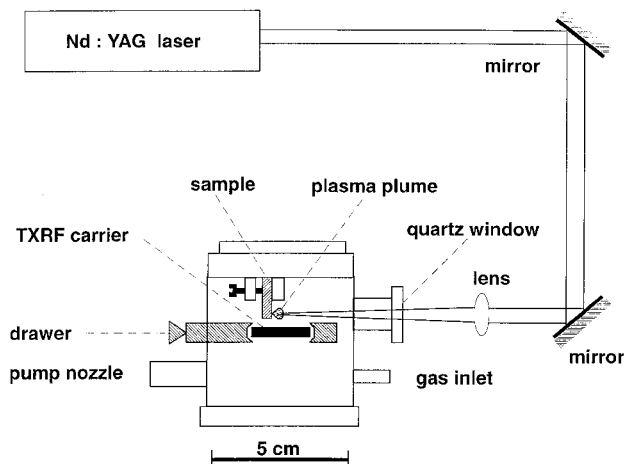


Fig. 1 Experimental arrangement for laser ablation and deposition of sample material on a TXRF carrier disc ( $x$ - $y$ - $z$  positioner not shown).

pressure was controlled by a capacitance pressure sensor (type Baratron 122AAX, MKS Instruments, Burlington, MA, USA) and adjusted by a needle valve in the by-pass circuit of the pumping line and by the flow rate of the argon gas ( $10$ – $110$  mL  $\text{min}^{-1}$ ). The chamber was moved *via*  $x$ - $y$ - $z$  translation stages which allowed micropositioning, in particular, of the height of the ablating laser beam above the TXRF carrier. The optically flat side of the carrier (diameter 30 mm, thickness 3 mm) was turned up to collect the ablated sample material. Plexiglas® discs were used mainly because they were equally suited but less expensive than quartz glass carriers. After deposition the chamber was ventilated slowly in order to prevent losses of deposited material.

For analysis, the carrier was taken out of the drawer and introduced into the TXRF instrument (Model EXTRA II, Rich. Seifert & Co, Ahrensburg, Germany). A Mo X-ray tube (50 kV, 38 mA) and an energy dispersive spectrometer equipped with a Si(Li) detector (Link QX 2000, Oxford Instruments, High Wycombe, Buckinghamshire, UK) were used. Spectra were recorded within a live time of 100 s. In order to obtain quantitative data, the method of internal standardization was applied. For this purpose 3  $\mu\text{l}$  of a standard solution containing 3 ng of Ge were added to the deposit by a pipette and carefully dried by infrared light. A more detailed description of the quantification approach was given in a previous paper.<sup>7</sup>

Most of the measurements were done on high-alloy steel, *i.e.* bulk sample H1, and a rolled steel sheet X5CrNi18 10, with low surface roughness (quality: polished roller). Analytical figures of merit were derived from a set of 14 samples of the binary system Fe–Cr. Samples used for this study and their composition are listed in Tables 1 and 2.

Table 1 Composition of the investigated steel samples in  $\text{mg g}^{-1}$

Element	Sample: H1 bulk sample	Sample: high-alloy steel sheet (X5CrNi18 10; trade name: V2A)
C	29	<0.5
P	2	
Si	115	
Mn	123	
Cr	116	180
Ni	43	100
Cu	37	
Ti	2	
W	51	
Fe	842	720

Table 2 Composition of Fe–Cr binary alloys

Sample No.	$c_{\text{Cr}}/\text{g g}^{-1}$	$c_{\text{Fe}}/\text{g g}^{-1}$
1	0	1
2	0.01	0.99
3	0.03	0.97
4	0.1	0.9
5	0.2	0.8
6	0.3	0.7
7	0.4	0.6
8	0.5	0.5
9	0.6	0.4
10	0.7	0.3
11	0.8	0.2
12	0.9	0.1
13	0.97	0.03
14	0.99	0.01

### 3 Results and discussion

The sample was mounted in an eccentric position of the sample chamber with a distance of 2 mm between sample surface and axis of the carrier (Fig. 1). To ensure that ablated material was deposited preferably in the central region of the TXRF carrier, *i.e.* in the visual field of the X-ray detector, the size of the laser plume and thus the spatial distribution of deposited material on the carrier had to be controlled. For this purpose the influences of laser pulse energy, argon gas pressure, argon flow rate and height of the ablating laser beam above the carrier were examined. The experimental parameters were optimized with respect to a maximum mass transfer rate defined below.

#### 3.1 Height of the ablating laser beam above the sample carrier

Fig. 2 shows a photograph of a typical laser plasma and schematically the arrangement of sample and carrier disc. In this case, the laser beam hits the sample at 2.5 mm above the carrier. The amount of deposited sample material was determined for different heights by means of the recorded TXRF intensities. Maximum amounts of Fe and Cr were detected for the binary sample No. 5 when the laser beam passed the surface of the carrier at a height of 1 mm. At this height the laser plume expanded just above the carrier. A smaller distance could not be applied due to partial screening of the laser beam. With increasing height up to some 3 mm the detected mass decreased continuously to about one-third of the maximum, indicating that in this case a significant amount of ablated material was deposited outside the visual field of the detector. In the present experiment the active area of the Si(Li) detector was 80  $\text{mm}^2$  and confined this field to a circular spot with 10 mm diameter on the carrier.

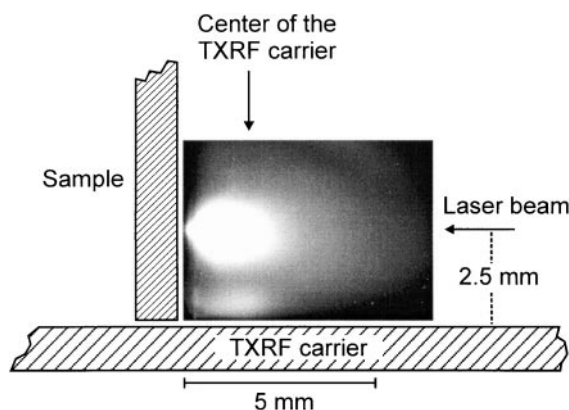


Fig. 2 Photograph of the laser plasma and schematic arrangement of sample and TXRF carrier disc.

### 3.2. Argon gas pressure and flow rate

To maintain a reproducible pressure setting in the ablation chamber the pumping speed of the vacuum pump was kept on a very low value by the needle valve in the by-pass circuit. The main pumping line was normally blocked during laser ablation and opened only for rapid evacuation of the chamber after replacement of carrier and sample. The actual gas pressure was adjusted by a defined flow rate of argon gas which was flushed continuously through the chamber. A working pressure of, for instance, 80 hPa was achieved with a moderate flow rate of 40 mL min<sup>-1</sup>. By means of this precaution, effects of the argon gas flow on the expansion of the laser plasma and thus on the distribution of the deposited material were minimized. The detected mass of material collected from the steel sample H1 as a function of the argon pressure is shown in Fig. 3. The maximum total amount of the Fe plus Cr deposit (37 ng) was observed for the lowest gas pressure applied (2 hPa), corresponding to a minimum flow rate of 1 mL min<sup>-1</sup>. With increasing gas pressure the total mass of the detected deposit decreased markedly and reached only 3 ng at pressure values > 100 hPa. The results indicated that the expansion of the laser plasma was hindered by the increasing pressure of the buffer gas. As a consequence, only a small fraction of ablated material reached the central area of the carrier disc, whereas a considerable amount was deposited outside the visual field of the TXRF detector or partially re-deposited on the sample due to collisions within the dense laser plasma.

### 3.3. Laser pulse energy and total number of laser shots

The nanogram amounts of analyte material required for a quantitative TXRF analysis were usually collected from 1–10 laser shots. Under these conditions the deposited mass increased linearly with the number of laser shots applied. With moderate laser energy ( $\approx 10$  mJ) and gas pressure (up to 50 hPa) a relatively large amount of ablated material was deposited in the central part of the carrier. With higher laser energy (> 15 mJ) the deposit covered a larger area of the carrier outside the visual field of the TXRF detector. For higher gas pressures (> 100 hPa), a partial absorption of laser radiation by a denser laser plasma had to be considered.<sup>11</sup> In this case the well known shielding effect reduced the laser radiation available for ablation.

In order to investigate the influence of the laser energy on the stoichiometric composition of the deposited sample material the pulse energy was varied between 10 and 40 mJ (Fig. 4). The mass ratio of the main constituents, Fe and Cr, in the deposit after ablation from high-alloy steel H1 was determined by TXRF and found to be close to the given value of 0.138. The results clearly demonstrated that the stoichiometric composition of the deposits was not affected by the laser energy if an

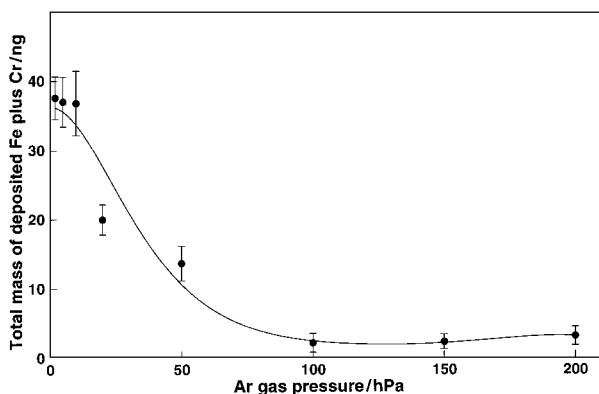


Fig. 3 Influence of the argon gas pressure on the total mass of the Fe plus Cr deposit detected by TXRF after ablation with ten laser shots from the steel sample H1. Laser pulse energy: 21 mJ.

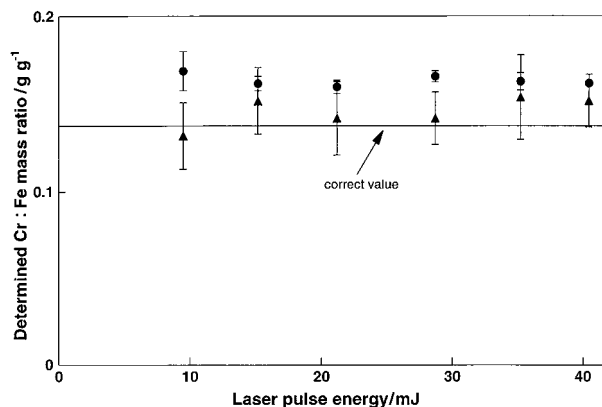


Fig. 4 Cr:Fe mass ratio of the deposit collected from steel sample H1 with ten laser shots versus laser pulse energy. Argon gas pressure: (●) 2 hPa, and (○) 140 hPa. The correct value for the mass ratio is 0.138.

adequate gas pressure of 50–80 mbar was chosen. At minimum pressure settings of 2 mbar, however, the measured Cr:Fe mass ratio increased slightly to 0.164. The excess of Cr cannot be explained by differences in vapour pressure because vapour pressures are nearly identical for Cr and Fe. The excess of Cr is presumably due to the lack of a sufficiently dense laser plasma which generally ensures that the different sample constituents are distributed equally in the laser plasma according to collision and diffusion processes. As a consequence, a gas pressure of about 80 mbar and a laser pulse energy of 15–21 mJ were chosen as optimum conditions for the following measurements.

### 3.4. Distribution of the deposited material

Apart from atomized matter the laser plume consists to a certain extent of microscopic particles such as clusters or aerosols. For qualitative inspection, the deposited sample material was investigated by techniques such as scanning electron microscopy, SEM, and electron probe microanalysis, EPMA.

Since the sample material collected from ten laser shots was not sufficient for SEM, about 200 shots were applied to obtain a visible pattern of the deposit. A rectangular piece of a Si wafer (15 × 15 mm<sup>2</sup>; 0.6 mm thick) with sufficient conductivity was used as a carrier instead of Plexiglas<sup>®</sup>, in order to prevent charging effects. Fig. 5(a) shows a deposit obtained from steel sample H1. A ring structure of about 5 mm diameter with a distinct zone of preferential deposition pointed towards the direction of the incoming laser beam. Since the diameter of the visual field ( $\approx 10$  mm) was larger than the diameter of the ring-shaped pattern, most of the deposited material was measured by the TXRF detector. A certain amount of non-atomized sample material was deposited in front of the sample surface below the laser crater. Scanning electron micrographs obtained at a higher resolution indicated that this deposit consisted mainly of micrometre-sized microscopic particles which could not penetrate into the dense laser plasma and consequently were not carried away. In contrast to the microparticles, the material deposited at the front of the plume formed a layer of clusters or particles of sub-micrometre size ( $\approx 60$  nm) as shown in Fig. 5(b). This layer possibly represents a vapour of analyte atoms which condensed during the cooling period of the initially hot laser plasma.

Obviously, the central area of the deposit was not covered by microscopic particles. This finding showed that the shock wave of the expanding laser plasma probably interacted with the deposit, in particular when the laser beam passed at minimum height (1 mm, see Fig. 2) and a larger number of laser shots were applied. EPMA measurements made on various microparticles resulted in Fe:Cr ratios which deviated by less than

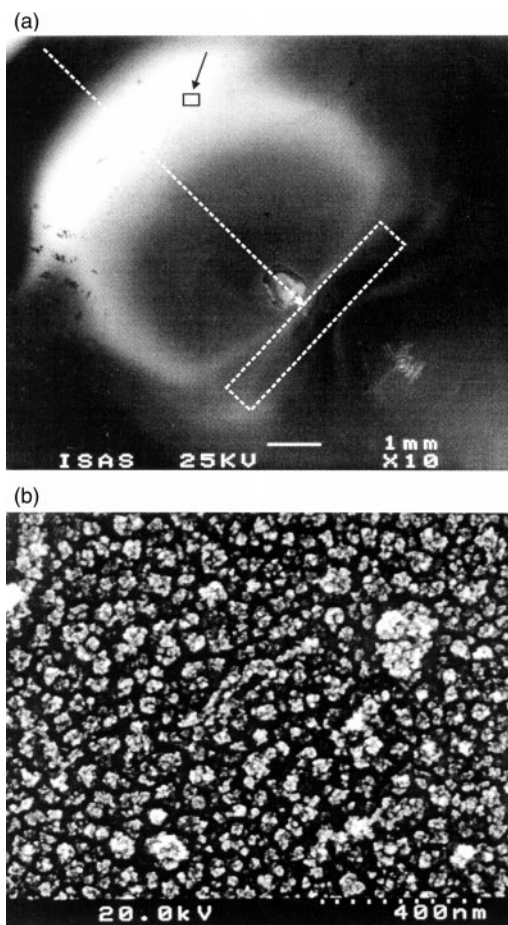


**Fig. 5** Scanning electron micrographs of the deposit collected on a Si wafer after ablation from the steel sample H1. A total of 200 laser shots of 21 mJ pulse energy were applied. Height of the laser beam above the sample surface: 1 mm. (a) Total view of the deposit. The position of the sample and the laser beam are shown schematically. Marked area represents the location shown in more detail in (b). (b) Ablated material deposited at the front of the laser plume [enlarged detail of (a)].

10% from the expected composition of the bulk sample. This confirmed clearly the absence of serious matrix effects during the processes of laser ablation and sample collection.

### 3.5 Mass transfer rate

A major goal of this study was to improve the transfer of ablated material to the carrier. As a figure of merit, the amount of material detected on the carrier was related to the total mass of ablated sample material. The ablated mass was determined either by the weight loss of the sample before and after ablation or by means of the geometrical dimensions of the laser crater, respectively. The crater dimensions after ablation with ten laser pulses of 25 mJ energy were obtained by optical microscopy. For a reliable calculation of the crater size, measurements were carried out on polished steel sheets with nearly optical surface quality. The ablated mass was 2  $\mu\text{g}$  with an estimated error of about  $\pm 0.2 \mu\text{g}$ , calculated from the optical measurements. The mass of the detected deposit was 25 ng on average, resulting in a mass transfer of 25 ng/2  $\mu\text{g}$ , *i.e.* about 1%. This result has to be compared with the value of 0.2% found for high-alloy steel in our previous experiments.<sup>7</sup> In spite of the uncertainty, the data indicated that the ratio of detected mass *vs.* ablated mass for the new arrangement of sample and carrier was improved by a factor of  $\approx 5$ . Since backscattering of ablated particles towards the sample was not taken into account, the optical measurements resulted in a mass transfer, which was certainly underestimated. In order to achieve more reliable results, re-deposition effects had to be considered. For this purpose the

mass loss after  $2 \times 10^3$  successive laser shots on small pieces of steel sheet (mass 3.0 g) was determined by means of an ultra microbalance (type UMT 5-Comparator; Mettler Toledo, Greifensee, Switzerland). To avoid crater effects during these measurements, 200 separate laser craters were formed by sets of ten laser shots each always on a fresh spot of the sheet. A total mass loss of 24  $\mu\text{g}$  was measured, corresponding to about 120 ng per ten laser shots on average. Basing the calculation on the 25 ng of deposited mass mentioned above, a mass ratio of detected *vs.* ablated mass of 25 ng/120 ng, *i.e.* 20% was estimated.

### 3.6 Analytical applications

**3.6.1 Iron–chromium binary alloys.** The analytical capabilities of the LA-TXRF technique were demonstrated on a set of 14 samples of Fe–Cr binaries (*cf.* Table 2). The TXRF spectra were recorded within 100 s live time which was adequate for the observed counting rates. For each measurement the material was removed from another sample spot and collected on a new carrier to repeat the complete process of quantification several times. The mass fractions obtained with ablation by a single laser shot are shown in Fig. 6 in relation to the expected or nominal values. The total amounts of Fe–Cr deposits detected by TXRF showed significant shot-by-shot fluctuations with a typical relative standard deviation, RSD, of about 0.15–0.25. The repeatability of the mass ratio, however, obtained for each sample was excellent as demonstrated by the error bars shown in Fig. 6. Each error bar represents the absolute standard deviation of the mass ratio of Fe and Cr derived from five replicates. It amounts to only 8  $\text{mg g}^{-1}$  on average. Moreover, determined and expected mass fractions agreed very well. The residual scatter of the mean values around the regression straight line is only 10  $\text{mg g}^{-1}$ .

From these experimental data the relative and absolute detection limits (LODs) were estimated. The corresponding blank values were derived from 20 independent measurements on carriers which had undergone all the different steps of the analytical procedure except for laser deposition, *i.e.* introduction into the sample chamber, evacuation, transport of the carrier into a clean bench, pipetting of the standard solution containing 3 ng of Ge, and finally TXRF measurement. On a  $3\sigma$  basis the absolute LODs derived for a single laser shot were 60  $\mu\text{g}$  for Fe and 50  $\mu\text{g}$  for Cr. Since typically a mass of 10 ng was collected from a single laser shot, relative LODs of 6  $\text{mg g}^{-1}$  for Fe and 5  $\text{mg g}^{-1}$  for Cr were obtained. To improve the detection power, more sample material had to be collected on the carrier. Therefore, in a second run of measurements, ten successive laser shots were applied to each

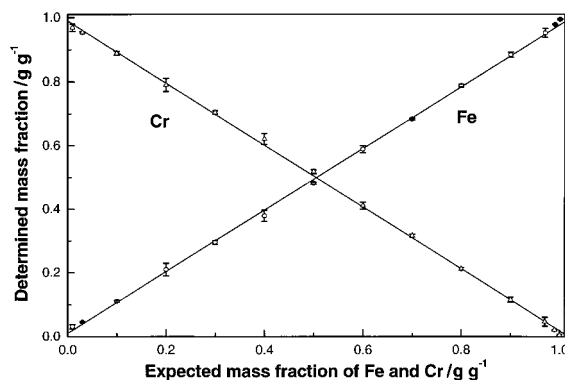


**Fig. 6** Mass fractions of Fe and Cr determined by LA-TXRF *versus* the mass fraction of both elements as expected from the known composition of the Fe–Cr binary samples. Material was collected by ablation with a single laser shot of 21 mJ pulse energy. Error bars represent the absolute standard deviation derived from five repetitive measurements. Prior to measurement each sample was treated with three laser shots without collecting a deposit.

Fe–Cr binary. The total mass of collected sample material was 60 ng and relative LODs of 1 mg g<sup>-1</sup> for Fe and 0.8 mg g<sup>-1</sup> for Cr were derived, sufficient for the determination of major and minor constituents in microsamples.

**3.6.2 Steel sheet.** In order to determine precision and accuracy of the LA-TXRF technique, an additional series of measurements was made with polished steel sheet (see Table 1). After ten laser shots of 21 mJ pulse energy the deposited masses of the main constituents were determined by TXRF. Twenty-five independent repetitive measurements led to the following average values and corresponding standard deviations: 20 ng for Fe ( $s = 5$  ng), 5 ng for Cr ( $s = 1$  ng), and 2.9 ng for Ni ( $s = 0.6$  ng). Consequently, the RSDs were between 0.20 and 0.25.

As far as the precision of analytical data is considered, the determination of mass fractions is to be preferred. The corresponding data obtained by LA-TXRF on a polished sheet of high-alloy steel were: 0.73 g g<sup>-1</sup> for Fe ( $s = 0.01$  g g<sup>-1</sup>), 0.168 g g<sup>-1</sup> for Cr ( $s = 0.008$  g g<sup>-1</sup>), and 0.106 g g<sup>-1</sup> for Ni ( $s = 0.005$  g g<sup>-1</sup>). The mean of the RSD values was only 0.04 (square root of the mean square of RSDs). Obviously, the determination of mass fractions was more precise than the measurement of absolute masses since fluctuations of the experimental parameters mentioned above were almost compensated for by internal standardization, *i.e.* ratioing of the relevant mass values. In contrast to the measurement of mass fractions, the data of absolute masses could not be corrected.

The accuracy of the mean values could be expressed by their relative deviations from the certified values: 0.01 for Fe, 0.07 for Cr and 0.06 for Ni. The mean of these values was 0.05. Consequently, precision and accuracy can be assumed to be sufficient for a micro-technique such as LA-TXRF.

**3.6.3 Non-metallic samples.** LA-TXRF has been applied so far to metallic samples such as Fe–Cr binaries and high-alloy steel. These materials are fairly homogeneous in chemical composition and can easily be ablated due to their high thermal conductivity. However, the advantages of laser sampling can be better demonstrated by the analysis of non-metallic materials such as ceramics, minerals or biological samples. Different components of minerals (inclusions or individual grains of a fragmented conglomerate) can be analyzed separately with moderate lateral resolution given by the size of the laser crater which had a diameter of typically 60 μm.

(i) *Aluminium–titanium ceramics.* Al and Ti were determined in a series of non-conductive sintered ceramic samples<sup>12</sup> which were mixed from powders of Al<sub>2</sub>O<sub>3</sub>, TiO<sub>2</sub> and SiO<sub>2</sub> according to the formal composition Si<sub>0.05</sub>(Al<sub>x</sub>Ti<sub>1-x</sub>)<sub>0.95</sub>O<sub>y</sub> ( $x$  varied in steps of 0.1 from 0.1 to 0.9). The substances were homogenized in a ball mill, pressed to pellets and sintered at temperatures above 1100 °C. In this case a tungsten X-ray tube was used for TXRF measurements because it was more appropriate for the excitation of aluminium than the Mo tube. Quantification was achieved through addition of 3 ng of scandium in the form of an acidic solution onto the deposit. Oxygen and silicon could not be determined under these conditions. Fig. 7 presents the results obtained for single shot ablation. As already observed for the Fe–Cr binaries, straight correlation lines were found also for Al–Ti ceramics.

(ii) *Mineral samples.* Geological materials usually consist of a large variety of mineralic phases with different chemical composition, crystal size and structure, and spatial distribution in the base material. As an example, the results of LA-TXRF analysis of natural granite are presented. The investigated material is known under the trade name ‘Rosa Sardo’ and originated from a mineral deposit in Spain. Although not required for LA, the samples were shaped (diameter ≈ 15 mm; thickness ≈ 4 mm) and polished for a better identification of

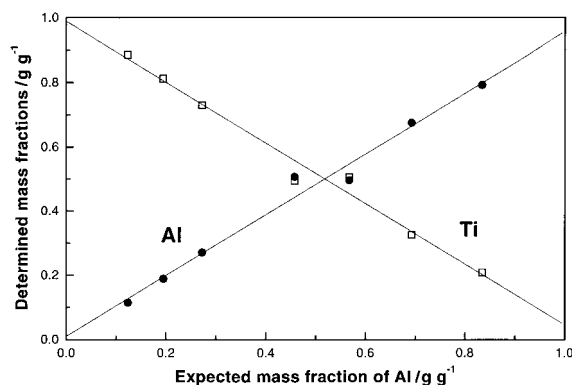


**Fig. 7** Mass fractions of Al and Ti determined by LA-TXRF versus mass fraction of aluminium known from the composition of the Al–Ti–Si oxide sintered mixtures. Material was collected from ablation by a single laser shot of 8 mJ pulse energy.

mineralic phases. Several different regions could be distinguished visually by their typical colours and were associated with the main mineralic compounds: white/brown—feldspar (calcite, albite, anorthite); grey—quartz; black—biotite (black mica).

Because of the poor thermal conductivity of the mineral samples about 20 laser shots were required to accumulate a deposit sufficient for TXRF analysis. Fig. 8(a) shows the TXRF spectrum obtained after ablation from the white zone, Fig. 8(b) the corresponding spectrum obtained from the black region of the granite. Since the latter was assumed to consist of biotite, it should have the following stoichiometric composition: [K,(Mg, Fe)<sub>3</sub>(OH, F)<sub>2</sub>(Al, Fe)Si<sub>3</sub>O<sub>10</sub>]. Accordingly, Fe and K were the dominating elements in the black material as shown in Fig. 8(b). The spectrum of Fig. 8(a) shows K and Ca as major elements. Their dominant presence is in accordance with the composition of different groups of feldspar which are described by the stoichiometry: [(Na, K)AlSi<sub>3</sub>O<sub>8</sub>] and [Ca(Al<sub>2</sub>Si<sub>2</sub>O<sub>8</sub>)].

As in previous measurements, Ge was added to the carriers as a standard. A complete quantitative analysis, however, was not possible since all light elements ( $Z < 14$ ) could not be detected by TXRF. Instead, the mass fractions of several typical elements, namely Ca, Ti, Fe and Rb, were determined, with the sum of the masses of the four elements set to 1 g g<sup>-1</sup>. Rb is a typical concomitant element of lepidolite, *i.e.* lithium mica, while Ti is always present in igneous rocks. Cu and Zn were not determined quantitatively since a blank signal of both elements could have been introduced by contamination from the ablation chamber which was made of brass.

In spite of the heterogeneous structure of the investigated samples, the analytical results obtained for a single mineralic

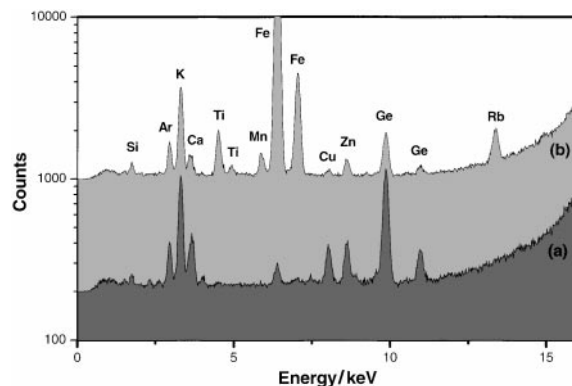


**Fig. 8** TXRF spectra of the deposit collected after ablation with 20 laser shots from different mineralic compounds of the granite sample ‘Rosa Sardo’. Laser pulse energy: 25 mJ. (a) Granite white; (b) granite black.

zone were fairly reproducible. Fig. 9 presents the results after sampling of four distinct black zones of the granite. Each series resulted from five repetitive measurements, applying 20 shots on the same sample spot. The mass fractions of the characteristic elements Fe, Ti and Rb varied with a RSD < 0.15. Only Ca as a ubiquitous element showed a much higher variation with a between-series RSD  $\approx$  0.45.

The assignment of mineralic phases to measured spectra may be difficult, if different modifications of a mineral are contributing to the recorded spectra. In this case a more sophisticated data evaluation is necessary such as cluster analysis.<sup>13</sup>

(iii) *Gallstones*. The gallstones investigated were from one person and varied in size from grains of sand to a jagged crystalline structure several millimetres in size. Owing to their hardness and colour the stones were of the so-called black type, *i.e.* pigment stones. For LA larger fragments of the gallstones were fixed to the sample holder by an adhesive tape. A spectrum obtained after ablation with a single laser shot is shown in Fig. 10. Obviously, Ca was the main element which forms crystalline sediments of calcium bilirubinate, a calcium compound of the gall pigment.<sup>14</sup> In addition to P, S, Cl and K, several heavier elements were identified such as Ti, Mn, Fe and Ni which were present in the gallstones within the range of about 5–20 mg g<sup>-1</sup> if related to the total mass of the detected elements. With ten measurements from different gallstone fragments, the following values for the RSD were obtained: 0.3 for Ca and about 0.6 for all the other elements mentioned above.

## Conclusion

The analytical capability of the LA-TXRF technique was investigated using an improved arrangement of sample and carrier. Compared with previous experiments the expansion of the laser plume was not obstructed by the TXRF carrier. In consequence, ablated material which had been collected already on the carrier was not removed by shock waves of successive laser pulses. The experimental parameters which determine the ablation process and the spatial distribution of material deposited on the carrier were investigated and optimized with respect to the mass of the collected deposit. A moderate laser pulse energy of 21 mJ was adequate to collect sample material sufficient to be easily analysed by TXRF. Maximum collection was found for a low argon gas pressure of 2 hPa, but a pressure of 50–80 hPa was preferred to ensure reproducible and accurate measurements.

The total mass of deposited material ablated by a single laser pulse was about 10 ng for the Fe–Cr binaries and > 40 ng for the ceramic samples investigated. The efficiency of mass

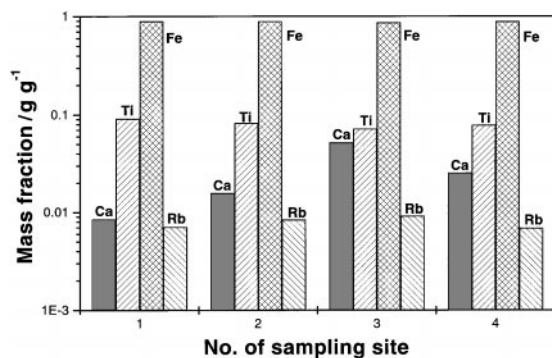


Fig. 9 Mass fractions of Ca, Ti, Fe and Rb determined by ablation with 20 laser shots from the black granite component of the rock sample 'Rosa Sardo'. The mass fractions were measured at four different surface spots and are presented on a logarithmic scale.

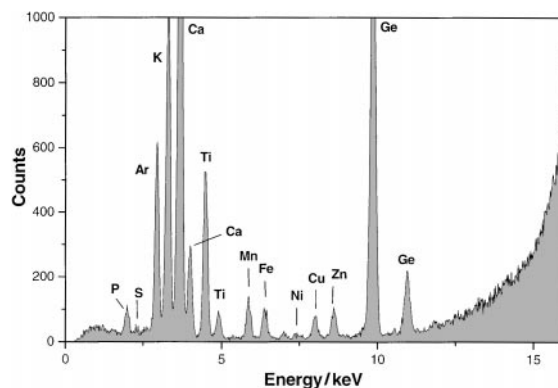


Fig. 10 TXRF spectrum of the deposit collected from gallstones by ablation with ten laser shots of 21 mJ pulse energy.

collection was considerably increased in comparison with previous experiments and estimated to be about 0.2. For single shot ablation from Fe–Cr binaries, the absolute LOD was 50–60 pg. Although different error sources might be relevant for the limited detection power, it may be assumed that the major influences are from the ablation process and the collection step coupled to it. The relative LOD for Fe and Cr of 5–6 mg g<sup>-1</sup> derived for single shot ablation is adequate for a rapid characterization of material by means of its major and minor components, but not for trace analysis.

In comparison with LA-ICP-MS, the combination of LA-TXRF is certainly less sensitive and the relative and absolute LODs are poorer by several orders of magnitude.<sup>15</sup> The advantage of LA-TXRF, however, is its easy and reliable quantification by internal standardization. This is important when a quantitative multi-element analysis by a single laser shot is required or solid reference materials are not available.

The lateral resolution of 50–100  $\mu$ m achieved with LA offers solid sampling from preselected spots of the specimen and thus the identification of different components in heterogeneous materials. Several metallic and non-metallic materials were investigated, thus demonstrating the analytical capabilities of LA-TXRF. This technique requires only nanogram amounts of material to be transferred to the TXRF carrier, avoiding any laborious and time consuming steps of sample preparation. The precision of LA-TXRF analysis was found to be satisfactory for micro- and local analysis. For metallic samples, for instance, the mass fractions were determined with a RSD of 0.05 whereas the detected masses varied by  $\approx$  0.25 due to shot-by-shot fluctuations. In order to prevent matrix effects and thus to improve the analytical accuracy, investigations with lasers with femtosecond pulse length are planned for the future. The ablation with femtosecond-laser shots is not dominated by thermal processes as with the nanosecond-laser and should therefore yield better reproducibility and accuracy.<sup>16,17</sup>

## Acknowledgements

The authors acknowledge the valuable experimental assistance of M. Schüth. They also thank M. Schlüter, Section Chemietechnik, University of Dortmund, for the scanning electron micrographs. This study was financially supported by the German Bundesministerium für Bildung, Wissenschaft, Forschung und Technologie and the Ministerium für Schule und Weiterbildung, Wissenschaft und Forschung des Landes Nordrhein-Westfalen.

## References

- 1 D. A. Rusak, B. C. Castle, B. W. Smith and J. D. Winefordner, *Trends Anal. Chem.*, 1998, **17**, 453.
- 2 R. E. Russo, X. Mao and O. V. Borisov, *Trends Anal. Chem.*, 1998, **17**, 461.

- 3 *Pulsed Laser Deposition of Thin Films*, ed. D. B. Chrisey and G. K. Hubler, Wiley, New York, 1994.
- 4 F. Leis, W. Sdorra, J. B. Ko and K. Niemax, *Mikrochim. Acta*, 1989, **II**, 185.
- 5 W. Sdorra, A. Quentmeier and K. Niemax, *Mikrochim. Acta*, 1989, **II**, 201.
- 6 W. Sdorra and K. Niemax, *Mikrochim. Acta*, 1992, **107**, 319.
- 7 S. Bredendiek-Kämper, A. von Bohlen, R. Klockenkämper, A. Quentmeier and D. Klockow, *J. Anal. At. Spectrom.*, 1996, **11**, 537.
- 8 R. Klockenkämper, in *Chemical Analysis—A Series of Monographs on Analytical Chemistry and its Applications*, ed. J. D. Winefordner, Wiley, New York, 1997, vol. 140.
- 9 R. Klockenkämper and A. von Bohlen, *J. Anal. At. Spectrom.*, 1999, **14**, 571.
- 10 X. L. Mao, A. C. Ciocan, O. V. Borisov and R. E. Russo, *Appl. Surf. Sci.*, 1998, **127–129**, 262.
- 11 J. A. Aguilera, C. Aragón and F. Peñalba, *Appl. Surf. Sci.*, 1998, **127–129**, 309.
- 12 H. Börner, H. Jenett and V.-D. Hodoroaba, *Fresenius' J. Anal. Chem.*, 1998, **361**, 590.
- 13 I. Bondarenko, B. Treiger, R. van Grieken and P. van Espen, *Spectrochim. Acta, Part B*, 1996, **51**, 441.
- 14 *Römpp Chemie Lexikon*, ed. J. Falbe and M. Regnitz, Georg Thieme, Stuttgart, 1990.
- 15 G. Tölg and R. Klockenkämper, *Spectrochim. Acta, Part B*, 1993, **48**, 111.
- 16 B. N. Chichkov, C. Momma, S. Nolte, F. von Alvensleben and A. Tünnermann, *Appl. Phys. A*, 1996, **63**, 109.
- 17 A. Rosenfeld, D. Ashkenasi, H. Varel, M. Wähmer and E. E. B. Campbell, *Appl. Surf. Sci.*, 1998, **127–129**, 76.